ACS SENSORS

pubs.acs.org/acssensors

Article

Near-Infrared Fluorescence Probe for Indication of the Pathological Stages of Wound Healing Process and Its Clinical Application

Xianzhu Luo,[+] Shaowen Cheng,[+] Wei Zhang,[+] Kun Dou, Rui Wang,* and Fabiao Yu*

Cite This: *ACS Sens.* 2024, 9, 810−819

Read Online

ACCESS | Metrics & More | Article Recommendations | Supporting Information

ABSTRACT: Chronic wound healing is one of the most complicated biological processes in human life, which is also a serious challenge for human health. During the healing process, multiple biological pathways are activated, and various kinds of reactive oxygen species participate in this process. Hydrogen peroxide (H_2O_2) involves in chronic wounds and its concentration is fluctuated in different pathological stages during the wound healing process. Therefore, H_2O_2 may be recognized as a powerful biomarker to indicate the wound healing process. However, the pathological roles of H_2O_2 cannot be fully understood yet. Herein, we proposed a near-infrared fluorescent probe DCM-H_2O_2 for highly sensitive and rapid detection of H_2O_2 in living cells and scald and incision wound mice models. DCM-H_2O_2 exhibited a low detection limit and high specificity with low cytotoxicity for H_2O_2, which had great potential for its application in vivo. The probe was successfully utilized to monitor the fluctuation of endogenous H_2O_2 in the proliferation process of human immortalized epidermal (HACAT) cells, which confirmed that H_2O_2 participated in the cells' proliferation activity through a growth factor signaling pathway. In the scald and incision wound mice models, H_2O_2 concentration fluctuations at different pathological stages during the wound healing process could be obtained by *in vivo* fluorescence imaging. Finally, H_2O_2 concentrations in different stages of human diabetic foot tissues were also confirmed by the proposed probe. We expect that H_2O_2 could be a sensitive biomarker to indicate the wound healing process.

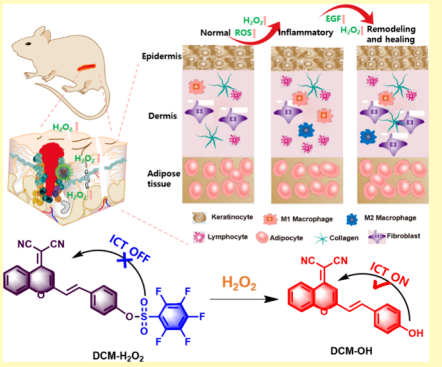

KEYWORDS: *near-infrared fluorescence imaging, hydrogen peroxide fluctuation, diabetes mellitus, wound healing, clinical sample test*

Chronic wound healing remains a global challenge and one of the major common public health problems that cannot be ignored.[1−3] It is a complex physiological process that consists of hemostasis, inflammation, proliferation and remodeling.[4,5] Unfortunately, bacterial infection or other diseases (destructive irrigation, diabetes mellitus) may interfere with wound healing, leading to impaired structural and functional regeneration of entire skin tissue, which in turn may lead to severe disability and even increased mortality.[6,7] Therefore, monitoring changes in physiological parameters during wound healing is crucial to understanding the state and physiological process of wound healing, which can help identify wound infections and subsequent treatment. The current clinical evaluation of wound healing mainly focuses on planimetry to quantitatively detect the changes of wound size and granulation tissue formation. Although this method can reflect the macroscopic changes in the wound, it cannot show regulation at the molecular level.

Excessive infiltration of neutrophils appears to be one of the culprits of chronic wound healing.[8] Abundant reactive oxygen species (ROS) in neutrophils is involved in all phases of wound healing, which can cause oxidative stress and adversely affect wound healing even prevent new tissue formation.[9−12] As a critical member of ROS, when hydrogen peroxide (H_2O_2) is generated at low concentrations (<0.7 μM) in a regulated fashion, it functions as a ubiquitous intracellular second messenger, which plays key roles in various physiological processes including cell growth, inflammation treatment, proliferation and differentiation, and activation of immune cells.[13−17] The previous researches indicate that H_2O_2, nitric oxide (NO), hypochlorous acid (HClO) involve in wound healing and its concentration is fluctuated in different pathological stages during the wound healing process.[18−25] While these studies are excellent, they are mainly focused on studies with zebrafish or tissue sections, and few studies have been used to detect changes in the levels of these substances during wound healing over a long period. Therefore, we attempted to monitor for a prolonged period of time the changes in H_2O_2 levels during wound healing in mice.

Although visual observation is the simplest and most versatile means of initial diagnosis of chronic wounds, it relies on the certain clinical experience and cannot predict the effect

Received: October 11, 2023
Revised: November 28, 2023
Accepted: December 29, 2023
Published: January 19, 2024

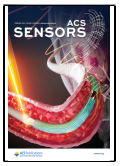

of treatment and the stage of healing.[26] Therefore, there is an urgent need to develop rapid and sensitive tools to detect H_2O_2 to accurately identify the various states of chronic wound healing.[27] Recently, fluorescent probes have been considered as powerful tools to monitor biological active species and processes due to their noninvasiveness, high sensitivity, and excellent spatial and temporal resolution.[28−34] Some fluorescent probes have been reported for monitoring H_2O_2 in living cells and *in vivo* through the careful design; however, the probes for monitoring the concentration fluctuation during the chronic wound healing process are still challenging.[35−39] Moreover, compared to the fluorescent emission in the visible light region, fluorescent probes with excitation/emission wavelength in the near-infrared (NIR) region get benefit from the low background interference, small light damage and deep penetration, which are more suitable for bioimaging.[40−42] With this in mind, we attempt to develop a NIR fluorescent probe for rapid and highly sensitive detection of H_2O_2 in living cells and *in vivo* to track the concentration fluctuations of H_2O_2 during chronic wound processes.

Herein, we proposed a NIR fluorescent probe DCM-H_2O_2 with a large Stokes shift for investigating the fluctuation of H_2O_2 level during chronic wound healing process in wound mice models and human diabetic foot tissues. The probe was comprised of a pentafluorobenzenesulfonyl ester group as recognition moiety of H_2O_2 and dicyanomethylene-benzopyran (DCM) as NIR fluorophore. In the presence of H_2O_2, DCM-H_2O_2 exhibited a rapid response to H_2O_2 with a large Stokes shift, emitting a brilliant fluorescent signal at 695 nm. Furthermore, DCM-H_2O_2 displayed a low cytotoxicity and excellent biocompatibility. Then, the proposed probe was applied to monitor the fluctuations of H_2O_2 level during the healing process of scald and incision wound mice models and in various pathological stages of the human diabetic foot, which contributed to comprehend the role of H_2O_2 in the physiological process. The probe could act as an effective tool to help diagnose the various stages of chronic wound healing that assist with further treatment.

EXPERIMENTAL SECTION

Synthesis of 1-(2-hydroxyphenyl)butane-1,3-dione (compound 2). 2-Hydroxybenzaldehyde (5 g, 41 mmol) was added to a round-bottom flask containing 60 mL of ethyl acetate. Then sodium metal (4 g, 174 mmol) was added, and the mixture was stirred at room temperature for 18 h. After the substitution reaction was completed, 5 mL of MeOH was added to completely react with the sodium metal. Then 50 mL of HCl (1 M) was added dropwise, and extracted with ethyl acetate, the organic phase was dried over Na_2SO_4. After removal of the solvent, compound 2 was obtained as a yellow solid, which was directly processed in the next step without treatment.

Synthesis of 2-methyl-4H-chromen-4-one (compound 3). Compound 2 and 1 mL of HCl were added to a round-bottom flask containing 50 mL of MeOH, and heated to reflux for 4 h. Then the solvent was removed, ethyl acetate was added, and the mixture was washed with saturated NaCl aqueous solution until colorless. After the solvent was removed, the residues were purified by silica column chromatography (200−300 mesh) with a gradient eluent of petroleum ether and ethyl acetate (10:1, v/v) to give a white solid (2.40 g, yield:75%). ^{1}H NMR (400 MHz, $CDCl_3$) δ (ppm): 8.17−8.15 (m, 1H), 7.62−7.60 (m, 1H), 7.36−7.36 (m, 2H), 6.16−6.15 (d, 1H), 2.37 (s, 3H).

Synthesis of 2-(2-methyl-4H-chromen-4-ylidene)-malononitrile (compound 4). Compound 3 (2.4 g, 15 mmol) and malononitrile (1.98 g, 30 mmol) were dissolved in 15 mL of acetic anhydride. The mixture was refluxed for 14 h, and then the solvent was evaporated in vacuum. Deionized water (80 mL) was added to the residue, and the mixture was refluxed for 0.5 h and then extracted with dichloromethane. The organic layer was dried using Na_2SO_4, filtered and concentrated. The resulting crude product was purified by silica gel column chromatography with a gradient eluent of CH_2Cl_2 to obtain an orange solid (1.28 g, yield: 41%). ^{1}H NMR (400 MHz, $CDCl_3$) δ (ppm): 8.91−8.88 (t, 1H), 7.73−7.69 (m, 1H), 7.46−7.42 (m, 2H), 6.70 (s, 1H), 2.43 (s, 3H).

Synthesis of (E)-2-(2-(4-hydroxystyryl)-4H-chromen-4-ylidene)malononitrile (DCM−OH). Under the protection of an Ar atmosphere, compound 3 (0.5 g, 2.4 mmol) and N-(4-formylphenyl)acetamide (0.25 g, 2 mmol) were added to 20 mL of acetonitrile, and 0.5 mL of piperidine and 0.5 mL of glacial acetic acid were added and refluxed for 4 h. A brownish red solid was precipitated and suction filtered to obtain crude product. The solid was washed with iced dichloromethane to obtain compound DCM−OH as a brown solid (0.28 g, yield: 46%). ^{1}H NMR (400 MHz, DMSO-d_6) δ (ppm): 8.73 (d, 1H), 7.91 (t, 1H), 7.79 (d, 1H), 7.70 (d, 1H), 7.61 (dd, 3H), 7.27 (d, 1H), 6.95 (s, 1H), 6.85 (d, 2H). ^{13}C NMR (100 MHz, DMSO-d_6) δ (ppm):160.1, 158.8, 152.7, 152.0, 139.2, 135.2, 130.3, 126.0, 124.6, 118.9, 117.4, 117.1 116.0, 115.8, 105.6, 59.0.

Synthesis of (E)-4-(2-(4-(dicyanomethylene)-4H-chromen-2-yl)vinyl)phenyl 2,3,4,5,6-pentafluorobenzenesulfonate (DCM-H_2O_2). The compound DCM−OH (0.31 g, 1 mmol) was dissolved in 10 mL of anhydrous tetrahydrofuran, and dimethylaminopyridine (0.30 g, 2.5 mmol) was added under Ar condition. The mixture was stirred at −10 °C for 20 min; pentafluobensulfonyl chloride (440 μL, 4 mmol) was added dropwise, and the mixture was stirred overnight at room temperature. A large amount of precipitation was separated out, filtered, and washed with dichloromethane to obtain DCM-H_2O_2. ^{1}H NMR (400 MHz, DMSO-d_6) δ (ppm): 8.75−8.73 (dd, 1H), 7.94−7.87 (m, 1H), 7.85−7.81 (d, 2H), 7.80−7.75 (m, 2H), 7.65−7.61 (m, 1H), 7.58−7.53 (d, 2H), 7.41−7.39 (d, 2H), 7.07 (s, 1H). ^{13}C NMR (100 MHz, DMSO-d_6) δ 158.0, 153.4, 152.5, 149.8, 137.0, 136.1, 135.7, 130.5, 126.8, 125.2, 123.2, 121.9, 119.6, 117.6, 117.5, 116.1, 107.9, 61.5. HR-MS, m/z calcd for $C_{26}H_{11}F_5N_2O_4S$, 542.0360; found $[M + H]^+$, 543.0436.

Cell culture and confocal imaging. Mouse monocyte-macrophage leukemia Cells (RAW 264.7 cells), human cervical cancer cells (HeLa cells), and human immortalized epidermal (HACAT) cells were incubated in DMEM supplemented with 10% FBS and 1% antibiotics (penicillin/streptomycin, 100 U/mL). The cultures were maintained at 37 °C in a 95% humidified atmosphere with 5% CO_2. Living cells were inoculated to a confocal plate and allowed to adhere for 24 h before imaging. Then, the probe (10 μM) was added before performing the imaging experiment. Red channel: λ_{ex} = 561 nm, λ_{em} = 650−730 nm, blue channel (DAPI): λ_{ex} = 405 nm, λ_{em} = 420−480 nm.

Fluorescent imaging of H_2O_2 in scald and incision mice wound model. All animal procedures were performed in accordance with the Guidelines for Care and Use of Laboratory Animals of Hainan Medical University and were approved by the Animal Ethics Committee of Hainan Medical University. In order to establish the mice model of scald and incision wounds, 12-week-old mice were selected as mice models. For the incision wound mouse model, we constructed a wound on the back of the mouse. In order to promote the healing of the wound and avoid the secondary injury caused by the mouse's activities, we sutured the wound through the surgery. For scalded mice, we used a sterilized metal rod to treat the back of the mice and established the related burn model. At different time points, the mice were imaged after the probe was sprayed for 60 min. The mice wound imaging were collected at 650−730 nm with λ_{ex} = 560 nm via PerkinElmer XR Series III System.

Clinical Sample Test. Human diabetic foot tissues were accessed from the First Affiliated Hospital of Hainan Medical University. The obtained tissues were stained with hematoxylin−eosin (H&E) to determine pathology. Furthermore, the fresh tissue sections were treated with the probe and then washed three times with PBS before

https://doi.org/10.1021/acssensors.3c02147
ACS Sens. 2024, 9, 810−819

fluorescence imaging. The Ethics Committee of Hainan Medical University approved this study.

RESULTS AND DISCUSSION

Design and synthesis of DCM-H_2O_2. In order to diagnose the various pathological stages of chronic wound healing by the dynamics of H_2O_2, it is necessary to develop rapid and highly sensitive H_2O_2 probes. Reasonable design of the probes is extremely critical for the specific detection of test substances in complex biological systems. The choice of NIR fluorophore plays key important roles for preparation of fluorescent probes that can be used in the wounds. DCM exhibits large Stokes shift, stable optical properties and NIR emission, which can be selected as the powerful fluorophore for the specific detection of H_2O_2.[43,44] Furthermore, the specificity of response groups toward H_2O_2 is one of the key parameters. Although a range of excellent borate-based fluorescent probes for hydrogen peroxide have been developed, their long reaction times make them unsuitable for rapid detection of changes in hydrogen peroxide levels.[45−47] Among the various response groups, the pentafluorobenzenesulfonyl group can rapidly and specifically recognize H_2O_2 without the significant interferences from other reactive oxygen species.[48,49] And the pentafluorobenzene ring increases the reactivity of sulfonates to H_2O_2, which may promote to enhance the probe's sensitivity to H_2O_2. Accordingly, the pentafluorobenzenesulfonyl group as the response group was introduced to develop the NIR fluorescent probe to track endogenous H_2O_2 fluctuations during the wound healing process. As expected, the pentafluorobenzenesulfonyl group exhibited high sensitivity, good selectivity, and rapid dynamics toward H_2O_2. Herein, a NIR fluorescent probe DCM-H_2O_2 triggered by H_2O_2 has been prepared through combining a DCM fluorophore and a pentafluorobenzenesulfonyl group (Scheme 1 and Figure S1). The equipment of response group

Scheme 1. Molecular structure of DCM-H_2O_2 and its proposed response mechanism towards H_2O_2

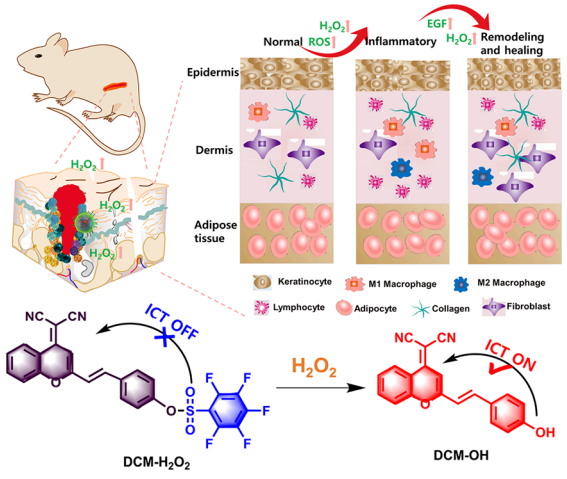

prevents the internal charge transfer (ICT) process of the fluorophore. In the presence of H_2O_2, the sulfonyl bond can be selectively removed, and then the free hydroxyl-fluorophore is released, which displays a characteristic fluorescence signal at around 695 nm. In order to further verify the release of DCM−OH,

Spectroscopic Properties of DCM-H_2O_2 toward H_2O_2. We discussed the spectral properties of the probe to determine whether DCM-H_2O_2 could be applied for the rapid detection of H_2O_2. The UV−vis absorption and fluorescence spectra of DCM-H_2O_2 were tested in PBS buffer solution (pH = 7.4, PBS: DMSO = 7:3, v/v). As illustrated in Figure 1A, DCM-

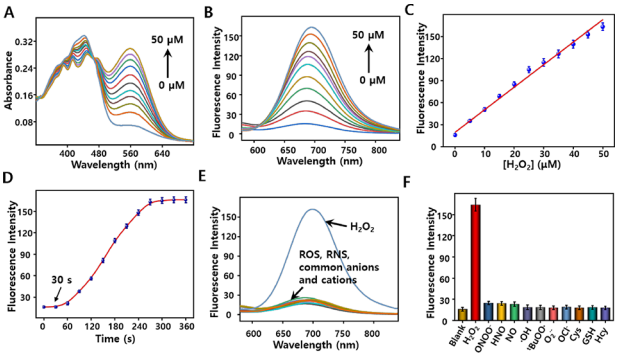

Figure 1. Spectral properties and selectivity of DCM-H_2O_2 (10 μM). (A) The UV−vis absorption spectra of DCM-H_2O_2 toward H_2O_2 (0−50 μM) for 5 min in PBS (pH = 7.4, 10 mM, PBS: DMSO = 7:3, v/v). (B) The fluorescence emission spectra of DCM-H_2O_2 toward H_2O_2 (0−50 μM) for 5 min in PBS (pH 7.4, 10 mM, PBS: DMSO = 7:3, v/v). (C) The linear relationship is between the fluorescence intensity of DCM-H_2O_2 and various levels of H_2O_2. (D) Time-dependent fluorescent intensity toward H_2O_2 during 0−360 s, and the probe was added at 30 s. (E) The fluorescence spectra of DCM-H_2O_2 toward other analytes, including ROS (50 μM, ·OH, $O_2^{\cdot-}$, OCl^-, and $^tBuOO\cdot$), RNS (50 μM, $ONOO^-$, NO, and HNO), common anions (1 mM, K^+, Na^+, Ca^{2+}, and Fe^{2+}) and cations (1 mM, Cl^-, Br^-, F^-, SO_4^{2-}, and CO_3^{2-}). (F) The fluorescent response of DCM-H_2O_2 to various reactive species at 10 min: 1. blank; 2. H_2O_2 (50 μM); 3. $ONOO^-$ (50 μM); 4. HNO (50 μM); 5. NO (50 μM); 6. ·OH (50 μM); 7. $^tBuOO\cdot$ (50 μM); 8. $O_2^{\cdot-}$ (50 μM); 9. OCl^- (50 μM); 10. Cys (200 μM); 11. GSH (200 μM); 12. Hcy (200 μM). The experiments were repeated three times, and the data were shown as mean (±S.D.).

H_2O_2 (10 μM) exhibited an outstanding absorption centered at 445 nm. After the addition of varied H_2O_2 levels (0−50 μM), there was a new absorption peak at around 560 nm and the absorption peak decreased successively at 445 nm, which indicated the generation of new compound after interacting with H_2O_2. Subsequently, the fluorescence response of DCM-H_2O_2 toward H_2O_2 was investigated. As the concentration of H_2O_2 increased, the fluorescence intensity gradually enhanced with strong emission at 695 nm under 560 nm excitation, which should be attributed to the interaction of the probe with H_2O_2, resulting in the dissociation of the pentafluorobenzenesulfonyl group on DCM-H_2O_2 (Figure 1B). Moreover, a good linear relationship between the fluorescence signals and H_2O_2 levels could be obtained with the range of 0−50 μM (Figure 1C). The regression equation was fitted as $F_{695\ nm} = 3.0684[H_2O_2] + 19.6552$ with a linear fitting constant of $R^2 = 0.9921$. Meanwhile, the limit of detection was determined as 64 nM according to the standard method of $3\sigma/k$.

Next, the reaction dynamics of DCM-H_2O_2 toward H_2O_2 was further accessed at 695 nm. As shown in Figure 1D, the fluorescence intensity increased sharply at about 2 min, reached a plateau at about 240 s, and remained stable in the presence of H_2O_2 (Figure 1D). These results indicated that the proposed probe displayed rapid response to H_2O_2, which attributed to the pentafluorobenzene ring increased the

https://doi.org/10.1021/acssensors.3c02147
ACS Sens. 2024, 9, 810−819

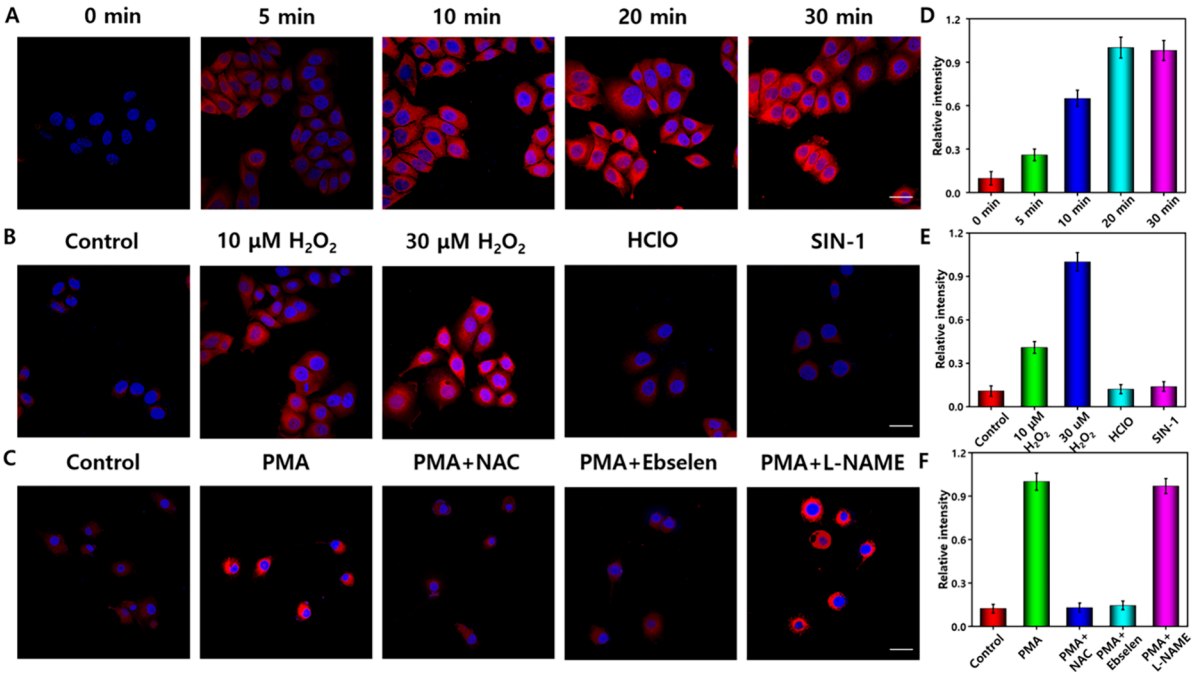

Figure 2. Fluorescence imaging of endogenous and exogenous H_2O_2 in living cells. (A) Fluorescent imaging of exogenous H_2O_2 in HeLa cells at different time points: 0 min, 5 min, 10 min, 20 and 30 min. (B) Fluorescent imaging of exogenous H_2O_2, HClO and $ONOO^-$ in RAW 264.7 cells. The RAW 264.7 cells were treated with H_2O_2 (10 μM, 30 μM), ClO^- and $ONOO^-$ donor (SIN-1), and then incubated with probe (10 μM), respectively. (C) Fluorescent imaging of endogenous H_2O_2 in RAW 264.7 cells. Control group: RAW 264.7 cells was incubated with the probe DCM-H_2O_2; PMA group: The RAW 264.7 cells were treated with PMA (1 μg/mL) for 6 h and then incubated with the probe DCM-H_2O_2; PMA + NAC group, PMA+ebselen, and PMA+L-NAME group: the cells were preincubated with NAC (1 mM), ebselen (5 μM), and L-NAME (5 mM) and then tread with probe, respectively. (D-F) Relative mean fluorescent intensities in A-C. Fluorescence collection windows for red channel: λ_{ex} = 561 nm, λ_{em} = 650−730 nm and blue channel (DAPI): λ_{ex} = 405 nm, λ_{em} = 420−480 nm. The experiments were repeated five times and the data were shown as mean (±S.D.). Scale bars: 20 μm.

reactivity of sulfonates to H_2O_2. The rapid response for H_2O_2 demonstrated that the probe showed great potential for the real-time imaging of H_2O_2 in complex biological systems. Moreover, excellent selectivity is essential to evaluate the probe's usability in the complexity of biological environment. The biological system contains a large number of reactive species as well as mercaptans, which may interfere with the detection of H_2O_2. As shown in Figure 1E and 1F, common active substances and biological mercaptans cannot cause apparent changes in the fluorescence signal after reaction including $ONOO^-$, ·OH, HNO, $^tBuOO\cdot$, NO, OCl^-, $O_2^{\cdot-}$, GSH, Cys, Hcy. Simultaneously, the common ions and anions including Fe^{2+}, Cu^{2+}, Ca^{2+}, Ba^{2+}, K^+, Na^+, Cl^-, I^-, Br^-, PO_4^{3-}, $S_2O_3^{2-}$, SO_3^{2-}, $S_2O_7^{2-}$, HS^-, AcO^-, SCN^-, HCO_3^-, NO_3^- could not induce the significant fluorescence signal changes (Figure S2). As expected, only H_2O_2 triggered a highly enhanced fluorescence signal since it could efficiently promote the release of the DCM−OH fluorophore, further demonstrating the excellent selectivity of DCM-H_2O_2 to H_2O_2.

The desirable fluorescent probe generally holds outstanding stability in the physiological pH range. We further discussed its effect on the probe in the pH range of pH 4.0−9.0. As shown in Figure S3, we found the fluorescence intensity of probe was basically constant, which indicated the high stability of the probe. In the presence of H_2O_2, the probe almost showed an inert fluorescent signal when the pH was less than 5. However, it exhibited brilliant fluorescence in a neutral environment, indicating that the probe might be employed to monitor H_2O_2 in biological systems. The data presented above demonstrated that the proposed probe DCM-H_2O_2 possessed great potential as a reliable chemical tool to measure the level of H_2O_2 in biological systems.

Imaging of H_2O_2 in living cells. In order to utilize the proposed probe to investigate the key role of H_2O_2 in chronic wound healing and to differentiate the physiological stages of wound healing, we set out to investigate whether the probe could be employed to monitor fluctuations in H_2O_2 in living cells. Herein, we first evaluated the cytotoxicity of the probe through a cell counting kit-8 (CCK-8). Three kinds of cells (HeLa cells, RAW 264.7 cells, and HACAT cells) were selected as cell models. As shown in Figure S4, the survival rates of these types of cells exceeded 80% even under high level of DCM-H_2O_2 (50 μM), indicating the low cytotoxicity of the probe.

Since the probe was provided with high sensitivity, good specificity, as well as low cytotoxicity, we hypothesized that DCM-H_2O_2 was able to detect H_2O_2 in living cells. Subsequently, we assessed the response time of the probe DCM-H_2O_2 in living cells. DCM-H_2O_2 was employed to detect and image exogenous H_2O_2 in HeLa cells (Figure 2A). The HeLa cells were first incubated with H_2O_2 and DCM-H_2O_2, then washed with PBS for three time before imaging. Herein, we chose different time points to perform imaging individually. The increased fluorescence single was found in HeLa cells within 5 min and reached saturation about 20 min. With the extension of time, the fluorescence intensity remains basically stable. Therefore, 20 min was selected as the optimal incubation time to perform the following experiments. Next, we investigated the ability of the probe to detect different concentrations of H_2O_2 and to discriminate among other

https://doi.org/10.1021/acssensors.3c02147
ACS Sens. 2024, 9, 810−819

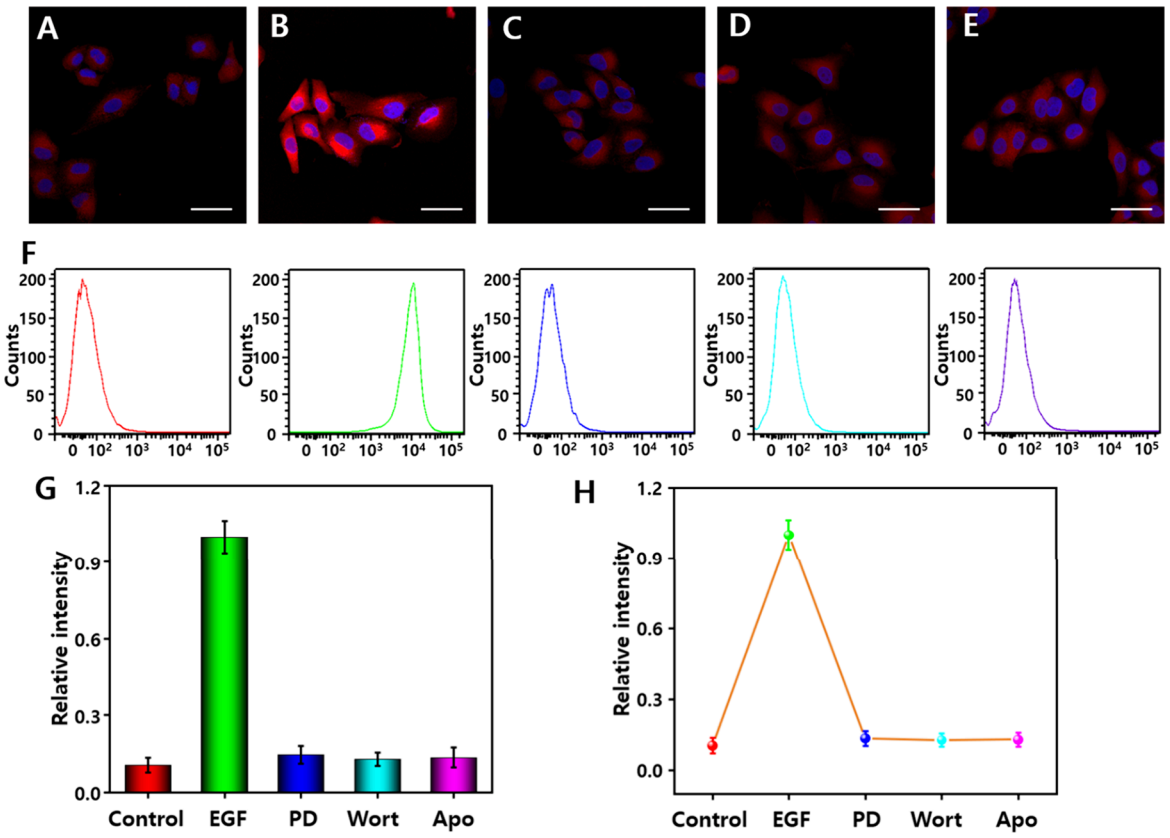

Figure 3. Fluorescence images and flow cytometry analysis of H_2O_2 in HACAT cells via DCM-H_2O_2. (A) The cells were treated with the probe DCM-H_2O_2 (10 μM). (B) The cells were incubated with EGF (500 ng/mL) for 30 min and then treated with probe. (C) The cells loaded with DCM-H_2O_2 were pretreated with PD153035 and then stimulated with EGF. (D) The cells loaded with DCM-H_2O_2 were pretreated with wortmannin and then stimulated with EGF. (E) The cells loaded with DCM-H_2O_2 were pretreated with apocynin before stimulated with EGF. (F) The flow cytometry analysis of the cells in A-E. (G) Relative mean fluorescent intensities in A-E. (H) Relative mean fluorescent intensities in F. The fluorescence collection windows for red channel (DCM-H_2O_2): λ_{ex} = 561 nm, λ_{em} = 650−730 nm and blue channel (DAPI): λ_{ex} = 405 nm, λ_{em} = 420−480 nm. The experiments were repeated five times, and the data are shown as mean (±S.D.). Scale bars: 20 μm.

species. Only weak fluorescence signal could be observed in HeLa cells after treatment with the probe for 20 min. In contrast, the cells were treated with 10 μM and 30 μM H_2O_2, respectively, and then incubated with DCM-H_2O_2 (10 μM), the enhanced fluorescence signals could be found, which indicated the proposed probe could detect H_2O_2 in living cells (Figure 2B). Next, we further investigated whether other reactive species could interfere the detection of H_2O_2 in living cells. The HClO and SIN-1 ($ONOO^-$ donor) were added to HeLa cells, respectively, and then these cells were incubated and imaged with DCM-H_2O_2. As we expected, no significant fluorescent signals could be obtained, which once again proved that the probe could specifically respond to H_2O_2 instead of other substances.

The practical usefulness of DCM-H_2O_2 for detecting and imaging endogenous H_2O_2 was further tested in RAW 264.7 cells. As well-known, the superoxide can be degraded to H_2O_2 by superoxide dismutase or through spontaneous dismutation. Moreover, the macrophages are able to generate superoxide under stimulation with phorbol-12-myristate-13-acetate (PMA).[50] The RAW 264.7 cells were treated with PMA (1 μg/mL) and then incubated with the probe DCM-H_2O_2. As shown in Figure 2C, PMA-stimulated RAW 264.7 cells revealed obvious fluorescence signal, while untreated RAW 264.7 cells only displayed weak fluorescence intensity. Nacetylcystein (NAC) serves as an efficient antioxidant that can scavenge H_2O_2 or inhibit its generation in living cells.[51] To verify the change of intracellular fluorescence intensity induced by the concentration fluctuations of endogenous H_2O_2, the cells were treated with NAC (1 mM) for 60 min before treated with PMA. The decreased fluorescent intensity was obtained, which confirmed that the fluorescence signal was caused by the endogenous H_2O_2. Then, the cells were treated cells with ebselen (5 μM), a mimic of H_2O_2 scavenger glutathione peroxidase, which exhibited the suppressed fluorescence intensity. L-NAME (5 mM) can inhibit the generation of · NO via nitric oxide synthase and then the conversion of NO to $ONOO^-$. However, after treatment with it, the fluorescence intensity basically remained stable, which demonstrated the intracellular fluorescence signal was indeed caused by the stimulation of H_2O_2 rather than other interferences. Taken together, the above results evidenced that the probe was able to visualize exogenous and endogenous H_2O_2 level in living cells, which provided strong evidence for further application in chronic wounds to detect dynamic changes in H_2O_2.

Imaging of H_2O_2 in HACAT cells. H_2O_2 is recognized as an essential signal molecule, which is inseparable from the process of cell proliferation and promotes the wound healing at the low concentration.[52] Here, we intend to study the fluctuation of H_2O_2 content during cell proliferation using human immortalized epidermal (HACAT) cells, which highly express horizontal epidermal growth factor receptor (EGFR)

https://doi.org/10.1021/acssensors.3c02147
ACS Sens. 2024, 9, 810−819

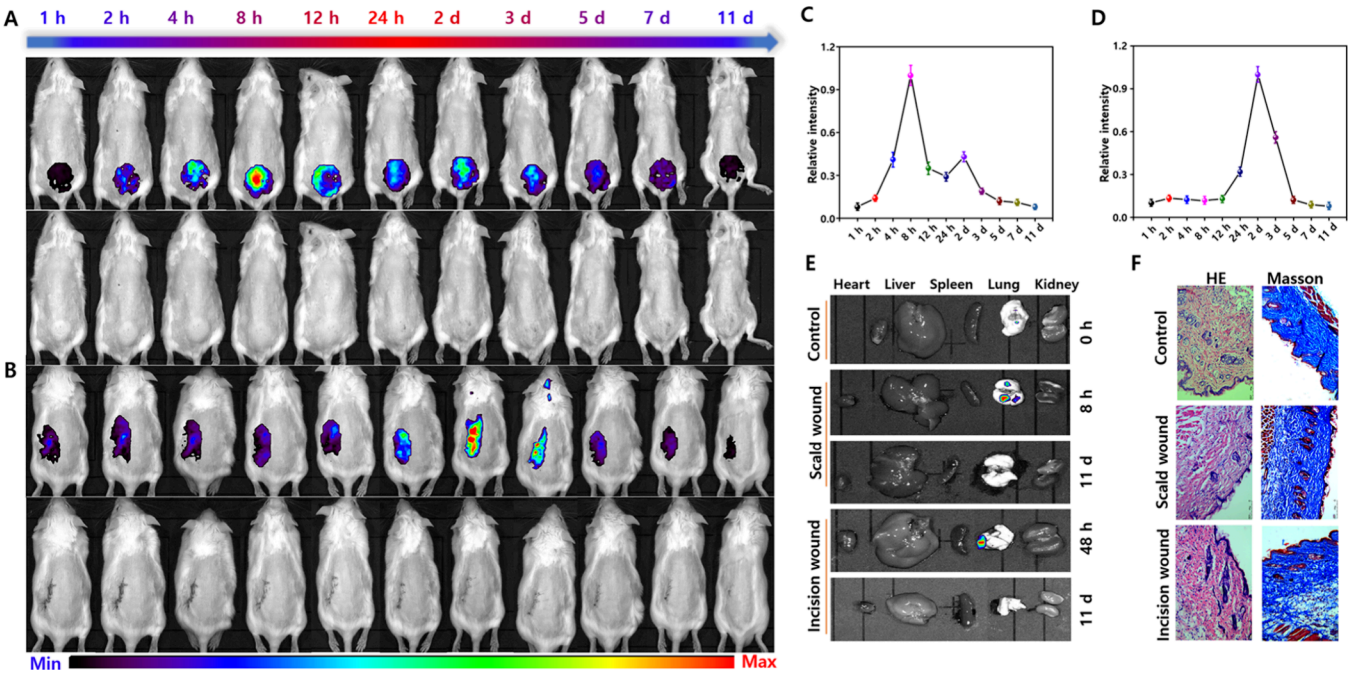

Figure 4. Time-dependent fluorescence images of H_2O_2 in wound healing models. (A) Fluorescence images of H_2O_2 with DCM-H_2O_2 in the healing process of the scald wound mouse model at different time points (1, 2, 4, 8, 12, 24, 2, 3, 5, 7, 7, and 11 d). (B) Fluorescence images of H_2O_2 with DCM-H_2O_2 in healing process of incision wound mouse model at different time points (1 h, 2 h, 4 h, 8 h, 12 h, 24 h, 2 d, 3 d, 5 d, 7 and 11 d). (C) Relative mean fluorescent intensities in A. (D) Relative mean fluorescent intensities in B. The fluorescence collection windows for red channel: λ_{ex} = 561 nm, λ_{em} = 650−730 nm. The experiments were repeated five times and the data were shown as mean (±S.D.). (E) The fluorescence detection of vitro vital organs (from left to right: heart, liver, spleen, lung, and kidney). (F) H&E and Masson staining for normal mice skin, period of inflammation of scald mice skin (8 h) and incision mice skin (48 h).

on the surface of the cell membrane.[53] Furthermore, EGF-stimulated HACAT cells transiently generate H_2O_2 by activating the Nox/PI3K pathway.[54] As control, the cells were only treated with DCM-H_2O_2, and a very weak fluorescent signal could be observed (Figure 3A). Subsequently, the HACAT cells were treated with EGF (500 ng/mL) and then stained using a probe (Figure 3B). As a result, enhanced fluorescence imaging was obtained, suggesting EGF treatment would induce a large amount of endogenous H_2O_2 production. To verify this result, we examined whether EGF could still cause significant changes in fluorescence signal by inhibiting EGFR. Here, PD153035 (an EGFR-specific inhibitor) was used to pretreat the cells before stimulation with EGF.[55] Thus, the weak signal indicated that PD153035 inhibited the binding of EGF to its receptor EGFR, which further implied that H_2O_2 was closely related to the growth and proliferation of cells (Figure 3C).

The upregulation of H_2O_2 levels in EGF-stimulated HACAT cells is attributed to activation of the Nox/PI3K pathway. In this pathway, as an important functional cellular enzyme, PI3K plays key role in cell growth, proliferation and differentiation.[56] We supposed that the activity of PI3K might affect the H_2O_2 concentration fluctuations. To verify the hypothesis, the HACAT cells were preincubated with an inhibitor of P13K, wortmannin, and EGF and subsequently stimulated the cells to observe fluctuations in peroxisome levels. As P13K was inhibited, the Nox/PI3K pathway could not be activated, allowing for slight fluctuations in H_2O_2 levels, while a weak fluorescent signal was correspondingly recorded (Figure 3D). Furthermore, similar experimental results were obtained when we treated with inhibitors of Nox (apocynin) (Figure 3E). The flow cytometry analysis was performed to check the above experimental phenomenon (Figure 3F). Furthermore, the relative mean fluorescence intensity of cell imaging exhibited a similar tendency with that of flow cytometry analysis (Figure 3G and 3H). These results indicated the important roles of H_2O_2 in cell growth and proliferation, which further illustrated that the proposed probe could be employed to track the concentration fluctuations of endogenous H_2O_2 and have the great potential to be utilized as the powerful biomarker to indicate the physiological stages of the wound healing process.

Imaging of H_2O_2 in scald and incision wound mice model. Since the probe can be successfully applied to highly sensitive and specific detection of endogenous H_2O_2 in cells, we tried to use it to track the concentration fluctuations of H_2O_2 during the wound healing process using DCM-H_2O_2. Here, we first constructed a scald model to study the concentration fluctuation of H_2O_2 during the wound healing process. A round wound with a diameter of 10 mm was constructed on the back of a female Balb/c mouse (18−22 g). The *in vivo* fluorescence imaging of the wounds on the back of the mice was performed at different time points after spraying the probe for 60 min within the range of 11 days. We found that the fluorescence intensity gradually increased with time and reached the maximum values at about 8 h after wound establishment (Figure 4A and 4C). The results implied a dramatic increase for H_2O_2 level in the early stage of wound healing phase, which could be attributed to the fact that the wounds experienced an inflammatory phase with a rise in cellular inflammatory factors and a burst of ROS, thus lead to an increase in H_2O_2 level and inhibited wound healing. Interestingly, the fluorescence intensity displayed a significant decrease at 12−24 h, indicating a decreased H_2O_2 concentration, which was attributed to the alleviation of the

https://doi.org/10.1021/acssensors.3c02147
ACS Sens. 2024, 9, 810−819

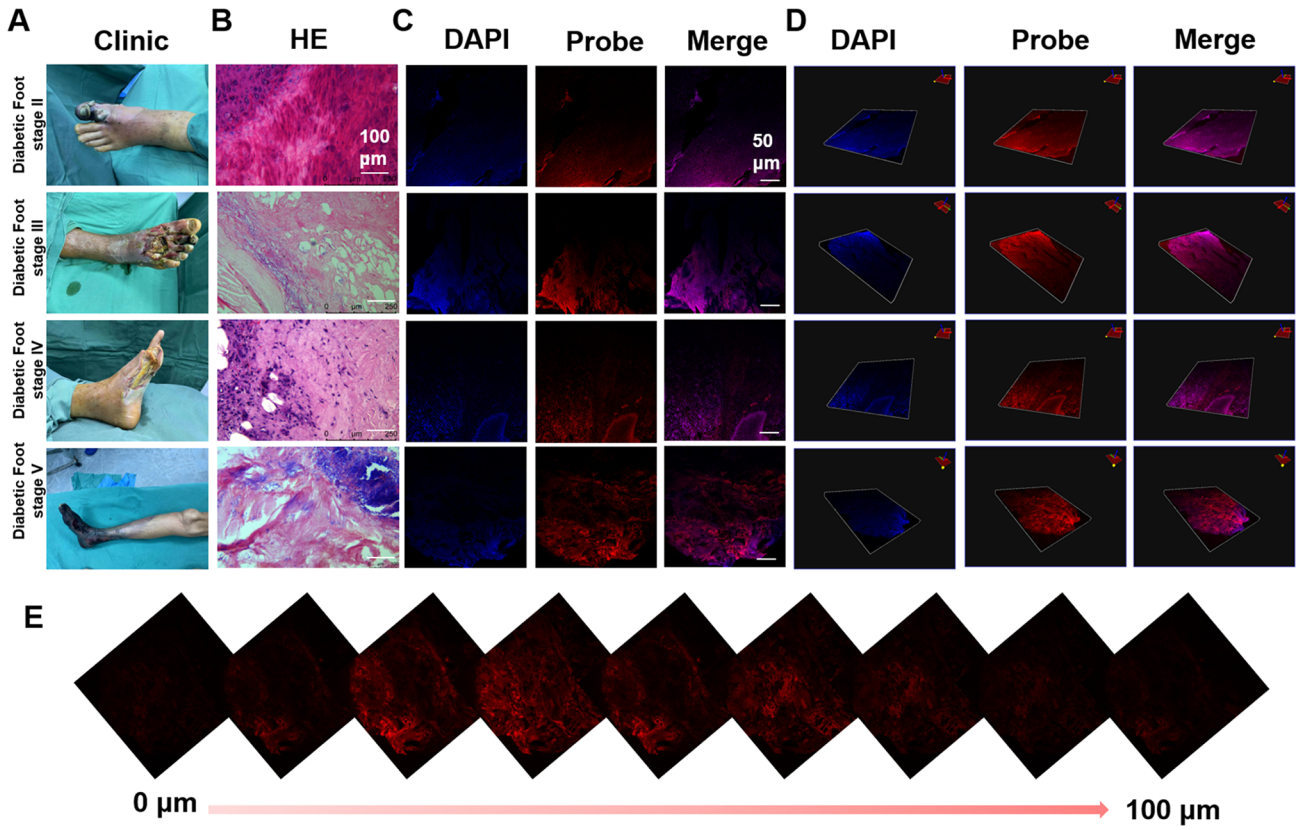

Figure 5. Fluorescent imaging in the tissues of the different physiological stages of the human diabetic foot. (A) Photographs of clinical samples. (B) H&E staining. Scale bars: 100 μm. (C) Fluorescence imaging of lesion skin tissues at lesion stages. The fluorescence collection windows for red channel: λ_{ex} = 561 nm, λ_{em} = 650−730 nm. Scale bars: 50 μm. (D) Three-dimensional (3D) images of (B). (E) Mapping of Z-line sequential images for a dysplasia slice at a depth interval of 10 μm (diabetic foot stage V).

inflammation at the scald wound of the mice. Due to the wound healing after 24 h until 11 days, the inflammation alleviated and H_2O_2 concentration decreased. At the inflammatory phase of wound healing, the increasing fluorescence intensity indicated that H_2O_2 played an indispensable role in cell growth and proliferation. Afterward, the wounds of the mice gradually healed completely, and the fluorescence signal was basically unchanged and remained at a weak level.

Encouraged by the above excellent results, we further investigated the concentration fluctuations of H_2O_2 during the incision wound healing process. We created a wound on the back of the female Balb/c mouse (18−22 g). The real-time fluorescence imaging was performed at different time points (1, 2, 4, 8, 12, 24, 2, 3, 5, 7, and 11 d) after treating with the probe for 60 min. As exhibited in Figure 4B and 4D, the fluorescence intensity of mice increased slightly at 2 h and reached the maximum at 2 d. Compared to the scald wound, the incision wound in deep tissues would require a longer duration of the inflammatory response. Wound healing was accelerated after the inflammatory response subsided, while the fluorescence signals decreased during 3−11 day, which demonstrated that our probe could track the concentration fluctuation of H_2O_2 during the incision wound healing process.

In addition, the oxidative stress states of the major organs including heart, liver, spleen, lung, and kidney were also checked through the fluorescence imaging of DCM-H_2O_2. As illustrated in Figure 4E, only the lungs exhibited a slightly increasing concentration of H_2O_2 in both the scald and incision wound mouse models, which indicated that the proposed probe could not affect the major organs. Furthermore, H&E and Masson staining of skin tissues of the wound mice models were utilized to further confirm the inflammatory states (Figure 4F). The healthy skin tissue was used as the control group. The staining results displayed slightly inflammatory cell infiltration and alveolar wall thickening with a small number of vacuoles forming, and relatively widespread collagen fiberd staining on the trabeculae. Simultaneously, no major damage was found in the heart, liver, spleen, lung and kidney (Figure S5). All the above results demonstrated that the proposed probe DCM-H_2O_2 could track the concentration fluctuations of H_2O_2 to indicate the wound healing progress, which had great potential to be used as a powerful tool to detect the H_2O_2 changes in the clinical samples, especially for the chronic wounds.

Imaging of H_2O_2 in clinical samples from wounds of diabetic patients. To further investigate the potential of DCM-H_2O_2 to discriminate the different stages of chronic wounds in clinical samples, we used the probe to monitor and image H_2O_2 in different diabetic foot stages. Herein, four different periods of human diabetic foot stages (II, III, IV and V stages) were selected (preidentified by pathological biopsy), and the skin tissues at the lesion sites were collected for testing (Figure 5A). H&E staining experiments were performed to confirm the pathological diagnosis (Figure 5B). The obtained fresh tissue sections were incubated with probe DCM-H_2O_2 for 30 min. Then, the sections were washed three times with PBS prior to fluorescence imaging. As shown in Figure 5C, the

https://doi.org/10.1021/acssensors.3c02147
ACS Sens. 2024, 9, 810−819

fluorescence intensities of tissue sections from four different pathological stages of diabetic foot patients were clearly different, which could be attributed to the chronic and sustained inflammatory state of diabetic patients, resulting in the corresponding upregulation of H_2O_2 levels. To highlight the imaging depth of the probe DCM-H_2O_2, we performed axial plane reconstruction of the three-dimensional (3D) image (Figure 5D and 5E). The probe could be fully penetrated and imaged in tissues of 100 μm thickness. The above results revealed that the probe possessed good penetration ability and could be used for H_2O_2 imaging in clinical diabetic diseases. The relevant levels of H_2O_2 in diabetic foot might serve as diagnostic indicators for the pathological stages of diabetic chronic wounds.

CONCLUSIONS

In summary, we reasonably designed and synthesized an NIR probe (DCM-H_2O_2) to track the concentration fluctuations of H_2O_2 during the scald and incision wound healing process and the human diabetic foot tissues. The probe exhibited high sensitivity and specificity and can respond quickly to H_2O_2. DCM-H_2O_2 was employed to detect exogenous and endogenous H_2O_2 and investigated the fluctuation of H_2O_2 during the proliferation of HACAT cells. Furthermore, the real-time imaging of H_2O_2 in the process of scald and incision wound mice models strongly demonstrated that the proposed probe could track the concentration fluctuations of H_2O_2 during the wound healing process. This study is helpful to better understand the role of H_2O_2 in the wound healing process. Furthermore, the probe was employed to image H_2O_2 in clinical diabetic foot samples, providing a new strategy for differentiating the pathological stages of diabetic foot.

ASSOCIATED CONTENT

Supporting Information

The Supporting Information is available free of charge at https://pubs.acs.org/doi/10.1021/acssensors.3c02147.

More experimental materials, general methods, synthesis routes, and compound characterization (PDF)

AUTHOR INFORMATION

Corresponding Authors

Rui Wang − *Key Laboratory of Hainan Trauma and Disaster Rescue, Department of Wound Repair, The First Affiliated Hospital of Hainan Medical University, Hainan Medical University, Haikou 571199, China; Engineering Research Center for Hainan Bio-Smart Materials and Bio-Medical Devices, Key Laboratory of Emergency and Trauma, Ministry of Education, Key Laboratory of Hainan Functional Materials and Molecular Imaging, College of Emergency and Trauma, Hainan Medical University, Haikou 571199, China*; Email: wangrui@hainmc.edu.cn

Fabiao Yu − *Key Laboratory of Hainan Trauma and Disaster Rescue, Department of Wound Repair, The First Affiliated Hospital of Hainan Medical University, Hainan Medical University, Haikou 571199, China; Engineering Research Center for Hainan Bio-Smart Materials and Bio-Medical Devices, Key Laboratory of Emergency and Trauma, Ministry of Education, Key Laboratory of Hainan Functional Materials and Molecular Imaging, College of Emergency and Trauma, Hainan Medical University, Haikou 571199, China*; orcid.org/0000-0003-0073-6299; Email: yufabiao@hainmc.edu.cn

Authors

Xianzhu Luo − *Key Laboratory of Hainan Trauma and Disaster Rescue, Department of Wound Repair, The First Affiliated Hospital of Hainan Medical University, Hainan Medical University, Haikou 571199, China; Engineering Research Center for Hainan Bio-Smart Materials and Bio-Medical Devices, Key Laboratory of Emergency and Trauma, Ministry of Education, Key Laboratory of Hainan Functional Materials and Molecular Imaging, College of Emergency and Trauma, Hainan Medical University, Haikou 571199, China*

Shaowen Cheng − *Key Laboratory of Hainan Trauma and Disaster Rescue, Department of Wound Repair, The First Affiliated Hospital of Hainan Medical University, Hainan Medical University, Haikou 571199, China*

Wei Zhang − *Key Laboratory of Hainan Trauma and Disaster Rescue, Department of Wound Repair, The First Affiliated Hospital of Hainan Medical University, Hainan Medical University, Haikou 571199, China; Engineering Research Center for Hainan Bio-Smart Materials and Bio-Medical Devices, Key Laboratory of Emergency and Trauma, Ministry of Education, Key Laboratory of Hainan Functional Materials and Molecular Imaging, College of Emergency and Trauma, Hainan Medical University, Haikou 571199, China*

Kun Dou − *Key Laboratory of Hainan Trauma and Disaster Rescue, Department of Wound Repair, The First Affiliated Hospital of Hainan Medical University, Hainan Medical University, Haikou 571199, China; Engineering Research Center for Hainan Bio-Smart Materials and Bio-Medical Devices, Key Laboratory of Emergency and Trauma, Ministry of Education, Key Laboratory of Hainan Functional Materials and Molecular Imaging, College of Emergency and Trauma, Hainan Medical University, Haikou 571199, China*

Complete contact information is available at: https://pubs.acs.org/10.1021/acssensors.3c02147

Author Contributions

[+]X.L., S.C., and W.Z. contributed equally to this work. X.L., S.C., and W.Z. did the formal analysis and investigation, designed and performed the experiments, performed validation, and wrote the original draft. K.D. developed the methodology and did the supervision and validation. R.W. and F.Y. performed the conceptualization, funding acquisition, methodology, validation, project administration, writing of the review, and editing

Notes

The authors declare no competing financial interest.

ACKNOWLEDGMENTS

This work was supported by the National Natural Science Foundation of China (No. 22264013, 22204037), Hainan Provincial Natural Science Foundation of China (No. 822MS174, 823QN245, 823MS050, ZDYF2021SHFZ238, ZDYF2022SHFZ288), Natural Science Research Talent Project of Hainan Medical University (Grant No. JBGS202101), Hainan Province Clinical Medical Center (2021), Hainan Province Clinical Medical Center and the Innovation Platform for Academicians of Hainan Province, Postgraduate Innovative Research Project of Hainan (HYYB2021A04), Nanhai Young-Talent Program of Hainan

(Grant No. 20202007), Project for Functional Materials and Molecular Imaging Science Innovation Group of Hainan Medical University.

■ ABBREVIATIONS

EGFR, epidermal growth factor receptor; H_2O_2, Hydrogen peroxide; HACAT, human immortalized epidermal; RAW 264.7 cells, mouse monocyte-macrophage leukemia cells; HeLa cells, human cervical cancer cells; ICT, internal charge transfer; PMA, phorbol-12-myristate-13-acetate; NAC, nacetylcystein; ROS, reactive oxygen species; NIR, near-infrared; DCM, dicyanomethylene-benzopyran; H&E, hematoxylin−eosin; CCK-8, cell counting kit-8

■ REFERENCES

(1) Gao, Y.; Nguyen, D. T.; Yeo, T.; Lim, S. B.; Tan, W. X.; Madden, L. E.; Jin, L.; Long, J. Y. K.; Aloweni, F. A. B.; Liew, Y. J. A.; Tan, M. L. L.; Ang, S. Y.; Maniya, S. D.; Abdelwahab, I.; Loh, K. P.; Chen, C. H.; Becker, D. L.; Leavesley, D.; Ho, J. S.; Lim, C. T. A flexible multiplexed immunosensor for point-of-care in situ wound monitoring. *Sci. Adv.* **2021**, *7*, No. eabg9614.

(2) Maleki, A.; He, J.; Bochani, S.; Nosrati, V.; Shahbazi, M. A.; Guo, B. Multifunctional Photoactive Hydrogels for Wound Healing Acceleration. *ACS Nano* **2021**, *15*, 18895−18930.

(3) Li, S.; Mohamedi, A. H.; Senkowsky, J.; Nair, A.; Tang, L. Imaging in Chronic Wound Diagnostics. *Adv. Wound Care* **2020**, *9*, 245−263.

(4) Guo, B.; Dong, R.; Liang, Y.; Li, M. Haemostatic materials for wound healing applications. *Nat. Rev. Chem.* **2021**, *5*, 773−791.

(5) Tan, D.; Zhu, W.; Liu, L.; Pan, Y.; Xu, Y.; Huang, Q.; Li, L.; Rao, L. In situ formed scaffold with royal jelly-derived extracellular vesicles for wound healing. *Theranostics* **2023**, *13*, 2811−2824.

(6) Xu, P.; Huang, W.; Yang, J.; Fu, X.; Jing, W.; Zhou, Y.; Cai, Y.; Yang, Z. Copper-rich multifunctional Prussian blue nanozymes for infected wound healing. *Int. J. Biol. Macromol.* **2023**, *227*, 1258−1270.

(7) Karamanou, K.; Perrot, G.; Maquart, F. X.; Brézillon, S. Lumican as a multivalent effector in wound healing. *Adv. Drug Delivery Rev.* **2018**, *129*, 344−351.

(8) Ding, Y.; Chen, Q. The NF-κB Pathway: a Focus on Inflammatory Responses in Spinal Cord Injury. *Mol. Neurobiol.* **2023**, *60*, 5292−5308.

(9) Wu, K.; Wu, X.; Chen, M.; Wu, H.; Jiao, Y.; Zhou, C. H_2O_2-responsive smart dressing for visible H_2O_2 monitoring and accelerating wound healing. *Chem. Eng. J.* **2020**, *387*, No. 124127.

(10) Tu, C.; Lu, H.; Zhou, T.; Zhang, W.; Deng, L.; Cao, W.; Yang, Z.; Wang, Z.; Wu, X.; Ding, J.; Xu, F.; Gao, C. Promoting the healing of infected diabetic wound by an anti-bacterial and nano-enzyme-containing hydrogel with inflammation-suppressing, ROS-scavenging, oxygen and nitric oxide-generating properties. *Biomaterials* **2022**, *286*, No. 121597.

(11) Chen, H.; Lin, S.; Zhang, D.; Xing, Y.; Yu, F.; Wang, R. Ratiometric SERS imaging for indication of peroxynitrite fluctuations in diabetic wound healing process. *Chem. Eng. J.* **2023**, *470*, No. 144024.

(12) Lin, S.; Chen, H.; Wang, R.; Jiang, T.; Wang, R.; Yu, F. Hollow silver−gold alloy nanoparticles for enhanced photothermal/photodynamic synergetic therapy against bacterial infection and acceleration of wound healing. *Biomater. Sci.* **2023**, *11*, 4874−4889.

(13) Rhee, S. G. Cell signaling. H_2O_2, a necessary evil for cell signaling. *Science* **2006**, *312*, 1882−1883.

(14) Sun, Y.; Han, L.; Strasser, P. A comparative perspective of electrochemical and photochemical approaches for catalytic H_2O_2 production. *Chem. Soc. Rev.* **2020**, *49*, 6605−6631.

(15) Guo, H.; Chen, G.; Gao, M.; Wang, R.; Liu, Y.; Yu, F. Imaging of endogenous hydrogen peroxide during the process of cell mitosis and mouse brain development with a near-infrared ratiometric fluorescent probe. *Anal. Chem.* **2019**, *91*, 1203−1210.

(16) Wen, Y.; Liu, K.; Yang, H.; Li, Y.; Lan, H.; Liu, Y.; Zhang, X.; Yi, T. A Highly Sensitive Ratiometric Fluorescent Probe for the Detection of Cytoplasmic and Nuclear Hydrogen Peroxide. *Anal. Chem.* **2014**, *86*, 9970−9976.

(17) Jing, X.; Peng, H.; Han, S.; Zhao, Y.; Lin, W. A multicolor reversible fluorescent probe for detecting SO_2 and H_2O_2: Revealing redox imbalance in ischemia-reperfusion model. *Sens. Actuators B* **2023**, *396*, No. 134615.

(18) Zhang, R.; Zhao, J.; Han, G.; Liu, Z.; Liu, C.; Zhang, C.; Liu, B.; Jiang, C.; Liu, R.; Zhao, T.; Han, M. Y.; Zhang, Z. Real-Time Discrimination and Versatile Profiling of Spontaneous Reactive Oxygen Species in Living Organisms with a Single Fluorescent Probe. *J. Am. Chem. Soc.* **2016**, *138*, 3769−3778.

(19) Mao, Z.; Jiang, H.; Li, Z.; Zhong, C.; Zhang, W.; Liu, Z. An N-nitrosation reactivity-based two-photon fluorescent probe for the specific in situ detection of nitric oxide. *Chem. Sci.* **2017**, *8*, 4533−4538.

(20) Mao, Z.; Ye, M.; Hu, W.; Ye, X.; Wang, Y.; Zhang, H.; Li, C.; Liu, Z. Design of a ratiometric two-photon probe for imaging of hypochlorous acid (HClO) in wounded tissues. *Chem. Sci.* **2018**, *9*, 6035−6040.

(21) Pham, D.; Basu, U.; Pohorilets, I.; St Croix, C. M.; Watkins, S. C.; Koide, K. Fluorogenic Probe Using a Mislow−Evans Rearrangement for Real-Time Imaging of Hydrogen Peroxide. *Angew. Chem., Int. Ed.* **2020**, *59*, 17435−17441.

(22) Niethammer, P.; Grabher, C.; Look, A. T.; Mitchison, T. J. A tissue-scale gradient of hydrogen peroxide mediates rapid wound detection in zebrafish. *Nature* **2009**, *459*, 996−999.

(23) Rabbani, P. S.; Abdou, S. A.; Sultan, D. L.; Kwong, J.; Duckworth, A.; Ceradini, D. J. In Vivo Imaging of Reactive Oxygen Species in a Murine Wound Model. *J. Vis. Exp.* **2018**, *17*, No. e58450.

(24) Pase, L.; Layton, J. E.; Wittmann, C.; Ellett, F.; Nowell, C. J.; Reyes-Aldasoro, C. C.; Varma, S.; Rogers, K. L.; Hall, C. J.; Keightley, M. C.; Crosier, P. S.; Grabher, C.; Heath, J. K.; Renshaw, S. A.; Lieschke, G. J. Neutrophil-Delivered Myeloperoxidase Dampens the Hydrogen Peroxide Burst after Tissue Wounding in Zebrafish. *Curr. Biol.* **2012**, *22*, 1818−1824.

(25) Hu, J.; Yang, R.; Qin, H.; Sun, Y.; Qu, L.; Li, Z. Spying on the Polarity Dynamics during Wound Healing of Zebrafish by Using Rationally Designed Carbon Dots. *Adv. Healthcare Mater.* **2021**, *10*, No. 2002268.

(26) Dong, R.; Guo, B. Smart wound dressings for wound healing. *Nano Today* **2021**, *41*, No. 101290.

(27) Huang, F.; Lu, X.; Yang, Y.; Yang, Y.; Li, Y.; Kuai, L.; Li, B.; Dong, H.; Shi, J. Microenvironment-Based Diabetic Foot Ulcer Nanomedicine. *Adv. Sci.* **2022**, *10*, No. 2203308.

(28) Yik-Sham Chung, C.; Timblin, G. A.; Saijo, K.; Chang, C. J. Versatile Histochemical Approach to Detection of Hydrogen Peroxide in Cells and Tissues Based on Puromycin Staining. *J. Am. Chem. Soc.* **2018**, *140*, 6109−6121.

(29) Li, S.; Huo, F.; Yue, Y.; Ma, K.; Wen, Y.; Yin, C. Distinguishable multi-substance detection based on three-channel NIR fluorescent probe in physiology and pathology of living cells and zebrafish. *Chin. Chem. Lett.* **2021**, *32*, 3870−3875.

(30) Dou, W. T.; Han, H. H.; Sedgwick, A. C.; Zhu, G. B.; Zang, Y.; Yang, X. R.; Yoon, J.; James, T. D.; Li, J.; He, X. P. Fluorescent probes for the detection of disease-associated biomarkers. *Sci. Bull.* **2022**, *67*, 853−878.

(31) Huang, Y.; Chen, W.; Chung, J.; Yin, J.; Yoon, J. Recent progress in fluorescent probes for bacteria. *Chem. Soc. Rev.* **2021**, *50*, 7725−7744.

(32) Verwilst, P.; Kim, H. S.; Kim, S.; Kang, C.; Kim, J. S. Shedding light on tau protein aggregation: the progress in developing highly selective fluorophores. *Chem. Soc. Rev.* **2018**, *47*, 2249−2265.

(33) Liu, W.; Chen, J.; Qiao, Q.; Liu, X.; Xu, Z. A TICS-fluorophore based probe for dual-color GSH imaging. *Chin. Chem. Lett.* **2022**, *33*, 4943−4947.

https://doi.org/10.1021/acssensors.3c02147
ACS Sens. 2024, 9, 810−819

(34) Liu, H.; Chen, L.; Xu, C.; Li, Z.; Zhang, H.; Zhang, X.; Tan, W. Recent progresses in small-molecule enzymatic fluorescent probes for cancer imaging. *Chem. Soc. Rev.* **2018**, *47*, 7140−7180.
(35) Yin, J.; Zhan, J.; Hu, Q.; Huang, S.; Lin, W. Fluorescent probes for ferroptosis bioimaging: advances, challenges, and prospects. *Chem. Soc. Rev.* **2023**, *52*, 2011−2030.
(36) Wang, W.; Jiang, W.; Liu, Y.; Li, Y.; Zhang, J.; Li, C. Near-infrared fluorescence probe with a large stokes shift for visualizing hydrogen peroxide in ulcerative colitis mice. *Sens. Actuators B Chem.* **2020**, *320*, No. 128296.
(37) Zhou, J.; Zhao, R.; Du, Y.; Liu, S.; Li, W.; Gai, S.; He, F.; Feng, L.; Yang, P. A Si-CdTe Composite Quantum Dots Probe with Dual-Wavelength Emission for Sensitively Monitoring Intracellular H_2O_2. *Adv. Funct. Mater.* **2022**, *32*, No. 2112083.
(38) Li, T.; Cao, K.; Yang, X.; Liu, Y.; Wang, X.; Wu, F.; Chen, G.; Wang, Q. An oral ratiometric NIR-II fluorescent probe for reliable monitoring of gastrointestinal diseases in vivo. *Biomaterials* **2023**, *293*, No. 121956.
(39) Ye, S.; Hu, J. J.; Yang, D. Tandem Payne/Dakin reaction: a new strategy for hydrogen peroxide detection and molecular imaging. *Angew. Chem., Int. Ed.* **2018**, *57*, 10173−10177.
(40) Luo, X.; Cheng, Z.; Wang, R.; Yu, F. Indication of dynamic peroxynitrite fluctuations in rat epilepsy model with a near-infrared two-photon fluorescent probe. *Anal. Chem.* **2021**, *93*, 2490−2499.
(41) Weng, J.; Wang, Y.; Zhang, Y.; Ye, D. An Activatable Near-Infrared Fluorescence Probe for in Vivo Imaging of Acute Kidney Injury by Targeting Phosphatidylserine and Caspase-3. *J. Am. Chem. Soc.* **2021**, *143*, 18294−18304.
(42) Xia, Q.; Feng, S.; Hong, J.; Feng, G. One probe for multiple targets: A NIR fluorescent rhodamine-based probe for $ONOO^-$ and lysosomal pH detection in live cells. *Sens. Actuators B Chem.* **2021**, *337*, No. 129732.
(43) Hou, T.; Cai, Y.; Zhang, Z.; Wang, C.; Tang, Y.; Zhu, M.; Wang, Y. Progress of Dicyanomethylene-4H-Pyran Derivatives in Biological Sensing Based on ICT Effect. *Front. Chem.* **2022**, *10*, No. 903253.
(44) Wu, X.; Shi, W.; Li, X.; Ma, H. Recognition moieties of small molecular fluorescent probes for bioimaging of enzymes. *Acc. Chem. Res.* **2019**, *52*, 1892−1904.
(45) Wu, L.; Tian, X.; Lee, D.; Yoon, J.; Lim, C.; Kim, H.; James, T. D. Two-photon ESIPT-based fluorescent probe using 4-hydroxyisoindoline-1,3-dione for the detection of peroxynitrite. *Chem. Commun.* **2021**, *57*, 11084−11087.
(46) Deng, Y.; Shi, X.; Hu, X.; Xu, L.; Liu, X.; Gao, G.; Wang, R.; Liang, G. A Chemiluminescent Probe for Imaging Peroxynitrite in Inflammatory Cells and Tissues. *Anal. Chem.* **2023**, *95*, 6496−6500.
(47) Shi, L.; Li, X.; Zhou, M.; Muhammad, F.; Ding, Y.; Wei, H. An arylboronate locked fluorescent probe for hypochlorite. *Analyst* **2017**, *142*, 2104−2108.
(48) Hu, L.; Liu, J.; Zhang, J.; Zhang, H.; Xu, P.; Chen, Z.; Xiao, E. A novel ratiometric fluorescent probe for rapid detection of hydrogen peroxide in living cells. *RSC Adv.* **2019**, *9*, 39532−39535.
(49) Maeda, H.; Fukuyasu, Y.; Yoshida, S.; Fukuda, M.; Saeki, K.; Matsuno, H.; Yamauchi, Y.; Yoshida, K.; Hirata, K.; Miyamoto, K. Fluorescent Probes for Hydrogen Peroxide Based on a Non-Oxidative Mechanism. *Angew. Chem., Int. Ed.* **2004**, *43*, 2389−2391.
(50) Larsen, E. C.; DiGennaro, J. A.; Saito, N.; Mehta, S.; Loegering, D. J.; Mazurkiewicz, J. E.; Lennartz, M. R. Differential requirement for classic and novel PKC isoforms in respiratory burst and phagocytosis in RAW 264.7 cells. *J. Immunol.* **2000**, *165*, 2809−2817.
(51) Zhang, W.; Huo, F.; Yue, Y.; Zhang, Y.; Chao, J.; Cheng, F.; Yin, C. Heat Stroke in Cell Tissues Related to Sulfur Dioxide Level Is Precisely Monitored by Light-Controlled Fluorescent Probes. *J. Am. Chem. Soc.* **2020**, *142*, 3262−3268.
(52) Bai, J.; Jiang, X. A facile one-pot synthesis of copper sulfide-decorated reduced graphene oxide composites for enhanced detecting of H_2O_2 in biological environments. *Anal. Chem.* **2013**, *85*, 8095−8101.
(53) Bos, M.; Mendelsohn, J.; Kim, Y. M.; Albanell, J.; Fry, D. W.; Baselga, J. PD153035, a tyrosine kinase inhibitor, prevents epidermal growth factor receptor activation and inhibits growth of cancer cells in a receptor number-dependent manner. *Clin. Cancer Res.* **1997**, *3*, 2099−2106.
(54) Dickinson, B. C.; Huynh, C.; Chang, C. J. A Palette of Fluorescent Probes with Varying Emission Colors for Imaging Hydrogen Peroxide Signaling in Living Cells. *J. Am. Chem. Soc.* **2010**, *132*, 5906−5915.
(55) Tang, B.; Yu, F.; Li, P.; Tong, L.; Duan, X.; Xie, T.; Wang, X. A near-infrared neutral pH fluorescent probe for monitoring minor pH changes: imaging in living HepG2 and HL-7702 cells. *J. Am. Chem. Soc.* **2009**, *131*, 3016−3023.
(56) Honnegowda, T. M.; Kumar, P.; Padmanabha Udupa, E. G.; Sharan, A.; Singh, R.; Prasad, H. K.; Rao, P. A comparative study to evaluate the effect of limited access dressing on diabetic ulcers. *Int. Wound J.* **2016**, *13*, 791−798.

https://doi.org/10.1021/acssensors.3c02147
ACS Sens. 2024, 9, 810−819